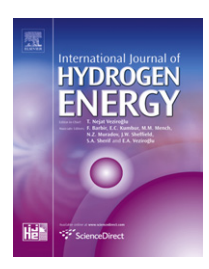


Available online at www.sciencedirect.com

SciVerse ScienceDirect

journal homepage: www.elsevier.com/locate/he



Synthesis and structural characterization of Co-doped lanthanum strontium titanates

F. Napolitano a, D.G. Lamas b, A. Soldati a, A. Serquis a,*

- ^a CONICET, Centro Atómico Bariloche, Av. Bustillo 9500, R8402AGP S.C. de Bariloche, Argentina
- ^b CONICET, Laboratorio de Caracterización de Materiales, Facultad de Ingeniería, Universidad Nacional del Comahue, Buenos Aires 1400, 8300 Neuguén, Argentina

ARTICLE INFO

Article history: Received 27 April 2012 Received in revised form 15 August 2012 Accepted 9 September 2012 Available online 5 October 2012

 $La_{0.4}Sr_{0.6}Ti_{1-y}Co_yO_{3+\delta}$

Crystal structure

Keywords: Symmetrical fuel cell electrodes

ABSTRACT

Lanthanum strontium titanates based oxides, materials with perovskite-type crystal structure, are good candidates for symmetrical fuel cell electrodes. They can become good mixed conductors (electronic and ionic) and reach adequate electrocatalytic activity for both oxygen reduction and fuel oxidation reactions if the right doping or structural modification of the (La,Sr)TiO3 compound is performed. However, the crystallographic information reported in the literature indicates a noticeable lack of reproducibility, since it is strongly dependent on synthesis conditions. In this work, $La_{0.4}Sr_{0.6}Ti_{1-v}Co_vO_{3+\delta}$ $(0.0 \le y \le 0.5)$ synthesis by a low-temperature chemical route and its structural characterization by X-ray powder diffraction and transmission electron microscopy are reported. From Rietveld refinements results, charge compensation mechanisms are studied and their correlation with synthesis parameters is discussed. We show that the creation of Sr vacancies at the A-site of the perovskite-type structure is the main compensation mechanism and their concentration decreases with the incorporation of Co in the crystal structure.

Copyright © 2012, Hydrogen Energy Publications, LLC. Published by Elsevier Ltd. All rights reserved.

1 Introduction

Fuel cells are electrochemical devices that convert chemical energy directly into electrical energy with high efficiency and low emission of pollutants. Hydrogen is normally used as the fuel and oxygen as the oxidant. However, solid-oxide fuel cells (SOFCs) are distinctive since they can operate with hydrocarbons as fuel, for instance methane, instead of hydrogen. Nevertheless, the requirement of high operating temperature (typically higher than 1073 K) implies great challenge for materials compatibility and stability leading to high manufacturing costs. The search for new cathode and anode

materials is oriented to achieve high electronic and ionic conductivities (i.e. 'mixed ionic-electronic conductors', MIECs), high electrocatalytic activity for oxygen reduction or fuel oxidation reactions, chemical stability with electrolyte and interconnection materials, thermal expansion coefficients compatible with that of the electrolyte, etc. In the case of the anode, an additional requirement is high performance with other fuels besides hydrogen (such as methane, natural gas, biogas, etc.) [1,2].

A new materials search branch has emerged recently from the Symmetrical Solid Oxide Fuel Cells (SSOFC) concept published by Ruiz-Morales et al. [3,4] where the same material is

^{*} Corresponding author. CONICET, Materials Characterization, Centro Atómico Bariloche, Instituto Balseiro, Av. Bustillo 9500, 8400 San Carlos de Bariloche, Rio Negro, Argentina. Tel.: +54 294 4445288; fax: +54 294 4445299.

E-mail address: aserquis@cab.cnea.gov.ar (A. Serquis).

used as anode and cathode simultaneously. This new approach could solve two of the main SOFCs problems, sulfur poisoning and carbon deposits when the cell is using hydrocarbon as fuel, by simply inverting the gas flux. Besides, this design should be less complicated than the conventional SOFCs due to the smaller number of components.

 $\text{La}_x \text{Sr}_{1-x} \text{TiO}_3$ (LST) has been widely reported as a possible SOFC anode material [2,5,6] and oxides based on this compound are also between the few reported as a possible electrode material for SSOFCs [7]. More generally, structural characterization of this compound has been reported in several articles with the common agreement that LST oxides have a cubic perovskite structure belonging to $Pm\overline{3}m$ space group for $x \leq 0.4$. However, lattice parameter evolution with La content (x) has been a major source of disagreement between all these works. It has been reported a decrease [8], as well as a slight [9] and even a strong [10] increment in the lattice parameter with x. This lack of reproducibility on its structural characterization was not explained until the correlation between structural parameters, charge compensation mechanisms and synthesis parameters was reported by Hashimoto et al. [11].

Proposed charge compensation mechanisms for LST are: perovskite A-site vacancy creation (at low temperature synthesis), perovskite B-site transition metal oxidation state changes (at high temperature synthesis and reductive atmospheres) or oxygen non-stoichiometry. A-site vacancies and oxygen rich phases are related through a structural reordering leading to a Ruddlesden-Popper phase [12] but evidences of this change (SrO characteristic planes) are difficult to acquire through conventional X-ray powder diffraction techniques [8,11]. Equation (1a) presents the A-site compensation mechanism while the 1b is the charge compensation one. However, the combination of 1a and 1b in Equation (2) reflects the relationship of A-site vacancies and transition metal oxidation state indicating that vacancies decrease when the amount of B_R' increases.

$$La_2O_3 + 2 Sr_{Sr}^x \leftrightarrow 2 SrO + 2 La_{Sr}^{\bullet} + V_{Sr}'' + O_O^x$$
(1a)

$$2 \operatorname{Ti}_{Ti}^x + O_O^x \!\leftrightarrow\! 2 \operatorname{Ti}_{Ti}' + V_O^{\bullet \bullet} + \frac{1}{2} O_2(g) \tag{1b}$$

$$2La_{Sr}^{\bullet} + V_{Sr}'' + 2Ti_{Ti}^{x} + 2SrO \leftrightarrow 2Ti_{Ti}' + V_{O}^{\bullet \bullet} + La_{2}O_{3} + 2Sr_{Sr}^{x} + \frac{1}{2}O_{2}(g) \quad (2)$$

On the other hand, through several experimental techniques a new explanation for La-doped Strontium Titanates structure has been reported by Canales-Vázquez et al. [13]. They discarded the A-site vacancies formation or Ti reduction mechanisms in favor of oxygen rich layered defects, based on the discovery of the new family of layered La-doped Strontium Titanates $\text{La}_4\text{Sr}_{n-4}\text{Ti}_n\text{O}_{3n+2}$. These ordered compounds were obtained via solid state reaction using high temperatures (up to 1873 K) and long time (up to 120 h) thermal treatments.

At SOFC cathode side, $La_xSr_{1-x}CoO_{3-\delta}$ is a well studied perovskite with excellent electrochemical properties that have turned it into one of the most successful SOFC cathodes until now [1]. Because SSOFC implicit design, its electrodes have to fulfill both SOFC anode and cathode requirements in the same material and, in this way, the substitution of Ti for Co in $(La,Sr)TiO_3$ is proposed in the present work. Oxygen ion

migration in $SrBO_3$ compounds has been calculated by Li et al. [14] using density-functional theory in the search of the best element for $SrTiO_3$ B-site doping. According to this work, the lowest oxygen ion migration energy corresponded to Sc, while Co resulted the second best for a 3d transition metal doping choice

Previous reports on $(\text{La,Sr})(\text{Ti,Co})O_3$ have been mostly related with their magnetic properties on epitaxially grown thin films [15,16] although some works have recently appeared in the fuel cells area: a small cobalt substitution in LST in order to obtain a good SOFC anode material was proposed by Yoo et al. [17] and Li et al. [18], while a Ti-doped SrCoO_3 cathode was presented by Shen et al. [19].

A complete structural characterization of SOFC electrodes is required for a comprehensive understanding of their electrochemical properties. For example, electrode properties are influenced by all charge compensation mechanism cited before: perovskite A-site vacancies affects the chemical compatibility with electrolyte and, together with oxygen vacancies, also the ionic conductivity; structural distortions (e.g. oxygen octahedral tilting) along with transition metal valence state are key factors for electronic conductivity [20]. In this work the synthesis of a new possible electrode material for SSOFCs based on $La_{0.4}Sr_{0.6}Ti_{1-\nu}Co_{\nu}O_{3+\delta}$ (LSTC) with $0.0 \le y \le 0.5$ oxides by a citrate chemical route and their structural characterization through synchrotron X-ray powder diffraction (XPD) is reported. Correlation between structural parameters, charge compensation mechanism and synthesis parameters is discussed.

2. Experimental

2.1. Synthesis

La_{0.4}Sr_{0.6}Ti_{1-y}Co_yO_{3+ δ} (0.0 \leq y \leq 0.5) (LSTC) powders were synthesized through a citrate chemical route based on Mao et al. [21] for BaTiO₃ synthesis. Precursor solution (0.1 M) was obtained by mixing stoichiometric amounts of tetrabutyl orthotitanate (\geq 97%, Fluka), SrCO₃ (99%, Alfa Aesar), Co(NO₃)₂·6H₂O (98%, Alfa Aesar), and La₂O₃ (99.99%, Alfa Aesar). First, 16% weight tetrabutyl orthotitanate was dissolved into ethylene glycol (99.9%, J. T. Baker) and stirred for 5 min until a clear solution was obtained. Then, 40% weight citric acid anhydrous (99.5%, Biopack) was added, at room temperature under continuous stirring, followed by deionizated water (15% weight) to help dissolving citric acid and to promote tetrabutyl orthotitanate hydrolysis reaction. Once the solution became clear again, La₂O₃, cobalt nitrate and SrCO₃ were incorporated directly, with a small amount of nitric acid (68%, Merk).

Precursor solution was then dried at 423 K in order to remove solvent excess and to promote polymerization until a solid resin was formed. Then, temperature was increased up to 573 K for charring this resin until an amorphous fine powder was obtained. From this powder, two separated series with different calcination temperature were then prepared: a high temperature series at 1373 K in order to obtain narrow peaks at XPD, and a low temperature series at 1123 K in order to study a nanostructured powder more functional for its application. For y=0.0 another sample (LSTcv) was prepared

in which A-site vacancies were taken into account in order to obtain the $\text{La}_x\text{Sr}_{1-3/2x}\text{TiO}_3$ composition. Table 1 summarizes the samples studied in this work and their nomenclature.

2.2. Characterization

LSTC structural characterization was performed by synchrotron XPD technique at the D10B-XPD beamline of the Brazilian Synchrotron Light Laboratory (LNLS, Campinas, Brazil) with a high-resolution configuration through a Ge(111) analyzer crystal and $\lambda=1.240232 \mbox{\normalfont\AA}$ (1373 K samples) [22], and also by inhouse XPD using a Philips PW1730/10 conventional diffractometer with Cu-K $_{\alpha}$ radiation (1123 K samples). Space group identification and Rietveld analysis [23] were carried out with Fullprof Suite software [24].

TEM and HR-TEM images were obtained using a Philips CM 200 UT microscope equipped with a LaB_6 filament operated at 200 keV and ultra-twin objective lens. The nominal resolution was 0.2 nm for high resolution mode. Particles were diluted in isopropanol, ultrasonicated for 5 min and deposited in Cu/hollow Carbon TEM grids. Bright field (BF), dark field (DF) and High Resolution (HR) images were digitally achieved using a CCD camera; contrast and illumination were adjusted linearly afterwards using commercially available image treatment programs.

3. Results and discussion

3.1. X-ray diffraction and structural parameters

 ${\rm La_{0.4}Sr_{0.6}Ti_{1-y}Co_yO_{3+\delta}}$ was successfully synthesized by a modification of a reported synthesis for ${\rm BaTiO_3}$ [21]. Our XPD analyses confirmed that the desired perovskite-type phase was obtained at 1123 K, 300 K lower than the synthesis temperature previously reported for a similar compound (synthesized through Pechini method) by Dwivedi et al. [25].

Fig. 1 shows diffractograms collected at LNLS from $La_{0.4}Sr_{0.6}Ti_{1-y}Co_yO_{3+\delta}$ samples with $0.0 \le y \le 0.5$ synthesized

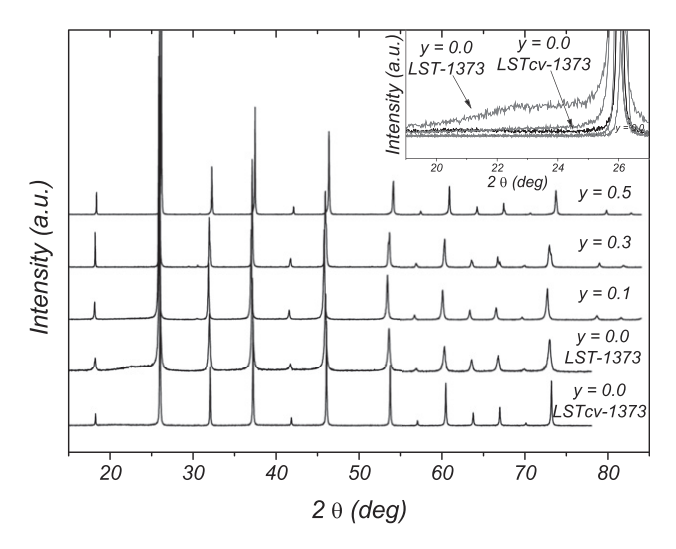


Fig. 1 — La_{0.4}Sr_{0.6}Ti_{1-y}Co_yO_{3+ δ} corresponding to 1373 K series difractograms acquired with synchrotron radiation ($\lambda=1.240232\text{Å}$). All reflections belong to perovskite phase. An increase is observed on background level for lower cobalt content samples (see details in inset).

at 1373 K, while equivalent results were obtained from 1123 K series, measured at our in-house diffractometer. The formation of the perovskite-type phase was confirmed for all compositions. LST samples were successfully identified with $Pm\overline{3}m$ cubic space group in agreement with previous works [9,26]. On the contrary, a low intensity peak at $2\theta=30.5^{\circ}$ (see Fig. 2a) and a splitting on several peaks were observed on Co-doped samples, indicating the loss of cubic symmetry and leading to $R\overline{3}c$ rhombohedral space group previously analyzed with DICVOL06 [27] and CHECKGROUP programs.

Nevertheless, Rietveld refinements using $Pm\overline{3}m$ space group have been performed resulting in worse Goodness of Fit (GOF) parameters. This result is opposed to the entry reported for LSTC oxides at the International Centre for Data Diffraction (ICDD) database where a $Pm\overline{3}m$ space group is reported

Table 1 $-$ La _{0.4} Sr _{0.6} Ti _{1-y} Co _y O _{3+δ} Rietveld refinements results and goodness of fit parameters. LSTcv-1373 sample was prepared taking into account perovskite A-site vacancies.								
Sample name	Nominal composition	T _{synthesis} (K)	Lattice parameter		Rp	Rwp	Re	χ^2
			a (Å)	c (Å)				
LST-1373	La _{0.4} Sr _{0.6} TiO ₃	1373	3.908 (2)		17.2 (*)	18.6 (*)	11.1	2.844
LSTC01-1373	$La_{0.4}Sr_{0.6}Ti_{0.9}Co_{0.1}O_3$	1373	5.5345 (8)	13.55616 (4)	9.98	12.5	10.2	1.480
LSTC03-1373	$La_{0.4}Sr_{0.6}Ti_{0.7}Co_{0.3}O_3$	1373	5.52119 (5)	13.4788 (2)	12.9	16.7	13.5	1.530
LSTC05-1373	$La_{0.4}Sr_{0.6}Ti_{0.5}Co_{0.5}O_3$	1373	5.46963 (4)	13.3766 (2)	18.8 (**)	24.9 (**)	15.5	2.590
LSTcv-1373	$La_{0.4}Sr_{0.4}TiO_3$	1373	3.89089 (2)		13.4	16.3	13.6	1.430
LST-1123	$La_{0.4}Sr_{0.6}TiO_3$	1123	3.8991 (2)		9.93	12.4	9.19	1.822
LSTC01-1123	$La_{0.4}Sr_{0.6}Ti_{0.9}Co_{0.1}O_3$	1123	5.5310 (9)	13.544 (4)	7.93	9.52	6.02	2.495
LSTC02-1123	$La_{0.4}Sr_{0.6}Ti_{0.8}Co_{0.2}O_3$	1123	5.5276 (2)	13.5561 (7)	8.70	11.0	7.28	2.288
LSTC03-1123	$La_{0.4}Sr_{0.6}Ti_{0.7}Co_{0.3}O_3$	1123	5.5249 (6)	13.529 (3)	7.08	8.63	5.68	2.307
LSTC04-1123	$La_{0.4}Sr_{0.6}Ti_{0.6}Co_{0.4}O_3$	1123	5.495 (1)	13.459 (5)	7.05	8.75	5.65	2.397
LSTC05-1123	$La_{0.4}Sr_{0.6}Ti_{0.5}Co_{0.5}O_3$	1123	5.476 (1)	13.41362 (6)	7.45	9.36	6.23	2.256

Note: Large Rwp and Rp values may be originated by (*) the increase on the background level and (**) a fault in the synchrotron line that produced a large asymmetry (too large axial divergence), but refined result values should not be affected by this problem.

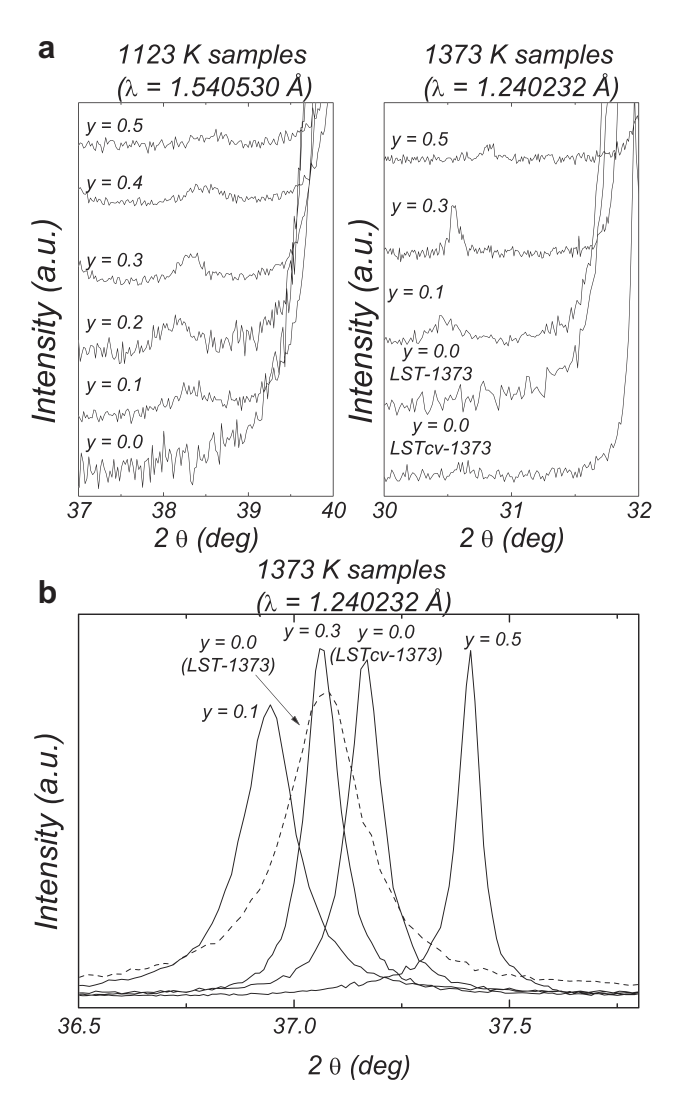


Fig. 2 — La $_{0.4}$ Sr $_{0.6}$ Ti $_{1-y}$ Co $_y$ O $_{3+\delta}$ diffractograms details corresponding to both samples series (sintered at 1123 and 1373 K) acquired using synchrotron radiation ($\lambda=1.240232\text{Å}$) with high resolution configuration and inhouse diffractometer with CuK α radiation ($\lambda=1.5418\text{Å}$). a) Rohmbohedral phase (113) reflection indicating Co-doped samples cubic structure symmetry loss. b) Rhombohedral phase (024) reflection position dependence with cobalt content.

but, in that work, only reflections with more than 10% of relative intensity were taken into account [25].

Fig. 2b shows (024) rhombohedral phase reflection position dependence with Co content while in Fig. 3 the Rietveld refinement result from a particular sample (LSTC03-1373) is displayed. A clear shift to higher angles is mainly observed for $y \geq 0.3$ samples, related with a decrease in the lattice parameter as will be discussed below.

LST samples exhibited an increase on the background level, mainly observed in the range $20^{\circ} \le 2\theta \le 26^{\circ}$ (Fig. 1 inset), which is independent of synthesis temperature. Explicitly, several heat treatments, 1223/1223/1323 K for 6 h each, were applied to the same sample and no change was observed on

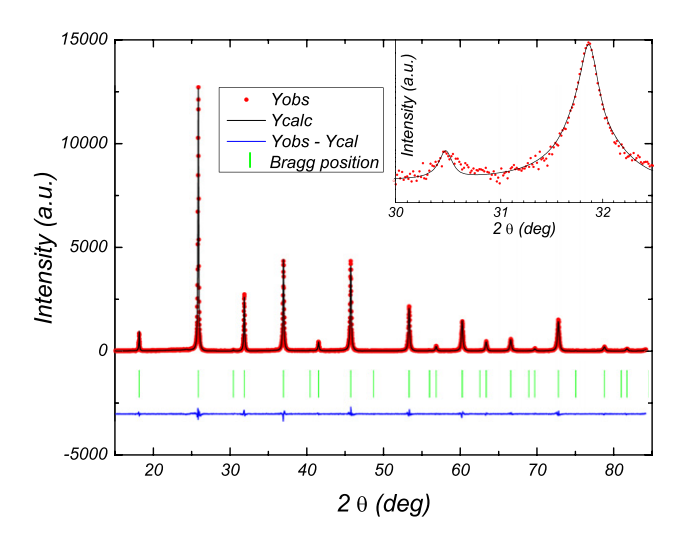


Fig. 3 – Rietveld refinement results on $La_{0.4}Sr_{0.6}Ti_{1-y}Co_yO_{3+\delta}$ with y=0.1 (1373 K sample XRD data, $\lambda=1.240232\text{Å}$). Rhombohedral distortion is detailed in inset (intensity in log scale).

background level (data not shown). A similar effect in the background was observed even using another synthesis route (based on acetic acid). This feature is responsible for the low goodness of fit obtained in Rietveld refinements for LST samples and may be attributed to the disorder caused by Sr segregation, as explained in the Introduction section. The existence of these disordered regions will be discussed in the next section (TEM observations). It is worth mentioning that this background level rapidly decreases with Co content and is absent on sample prepared taking into account compensated vacancies (LSTcv-1373).

Evolution of the LSTC lattice parameter of the cubic structure (y=0.0) and pseudocubic equivalent ($y\geq0.1$) with Co content is displayed in Fig. 4. Samples with Co

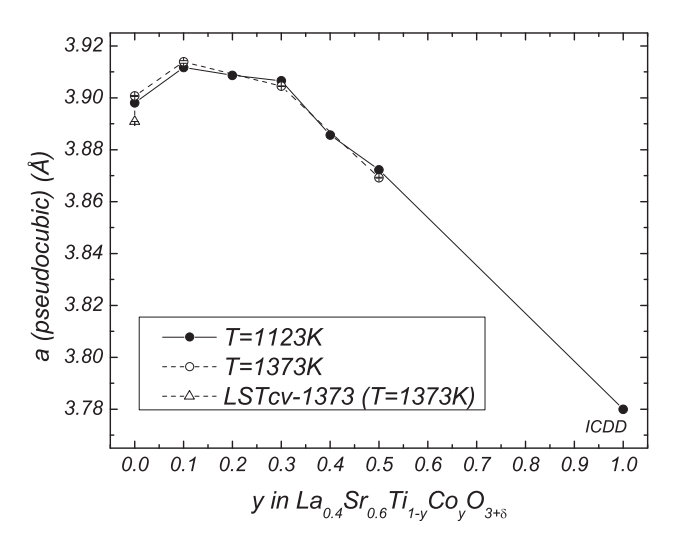


Fig. 4 – Lattice parameter as a function of cobalt content (y) in $\text{La}_{0.4}\text{Sr}_{0.6}\text{Ti}_{1-y}\text{Co}_y\text{O}_{3+\delta}$ calculated from Rietveld refinements (y=1.0 value obtained from ICDD database PDF [28]). Error bars are the size of the symbols.

concentration between 0.0 and 0.3 show a relatively stable value, then it linearly decreases towards $La_{0.4}Sr_{0.6}CoO_3$ value [28] for y > 0.3. This variation corresponds to the position shift of the (024) reflection followed in Fig. 2. No significant changes are observed between samples synthesized at different temperatures, but a notable difference is obtained between LST-1373 and LSTcv-1373 samples.

Changes in the Ti oxidation state (from +4 to +3) are possible if high temperature and a reducing atmosphere are used during the synthesis [10]. Since none of these conditions were employed in the present work, LST samples are expected to be on the left side of Equation (2) and a structure with cationic vacancies with general formula La_xSr_{1-3/2x}TiO₃ is reached. Perovskite A-site vacancies concentrations were calculated through Rietveld refinement by means of strontium occupancy parameter. Sr concentration values near theoretical 0.4 were obtained for LST with Lanthanum content of x = 0.4 supporting the model of perovskite A-site vacancy creation as the system dominant charge compensation mechanism. This result is in agreement with Hashimoto et al. for low temperature synthesis and with their theoretical value for LST structures with cationic vacancies, as previously stated. We are not considering the formation of some of the layered perovskite family La₄Sr_{n-4}Ti_nO_{3n+2} members reported by Canales-Vázquez because of n value inconsistency: for a sample with La:Sr = 1:1 ratio corresponds n = 8 while n = 10is the right value for La:Ti = 4:10. Furthermore, no evidences of extra peaks corresponding to the reported n = 8 and n = 10were observed in our high resolution XRD and no layered defects were observed in our HRTEM images (see next section). This difference could be explained due to different synthesis routes, i.e. our samples were prepared at lower temperature (1123-1373 K), while samples studied by Canales-Vázquez et al. were prepared at temperatures over 1673 K favoring the ordered phases.

Substitution of Ti with Co was performed aiming to evaluate its effect over electric and electrocatalytic properties as SSOFC electrode, which will be reported elsewhere. This substitution add one term in charge compensation Equation (2) corresponding to Co oxidation state change. When Co proportion is increased, the charge compensation mechanism is expected to change from 'A-site vacancies creation' to 'Bsite transition metal oxidation state change' because Co is more susceptible than Ti to modify its oxidation state. Fig. 5 shows Sr concentration evolution with Co content. A remarkable Sr increment between $0.0 \le y \le 0.3$ is observed, tending to the stoichiometric theoretical value of 0.6. The main difference between both samples series (1123 and 1373 K) is that the stoichiometric value is actually reached only by the high temperature series. This is due to the higher energy available during the synthesis process, which allows shifting to other compensation mechanisms even with lower Co proportions.

The range with steady lattice parameter is coincident with the range where A-site vacancies creation charge compensation mechanism is active and still dominant (Fig. 5), indicating a correlation between them.

Fig. 6a shows the structure distortion level on Co-doped samples through oxygen octahedra tilt angle (TM - O - TM angle), where a clear shift from the ideal 180° is noted. A slight

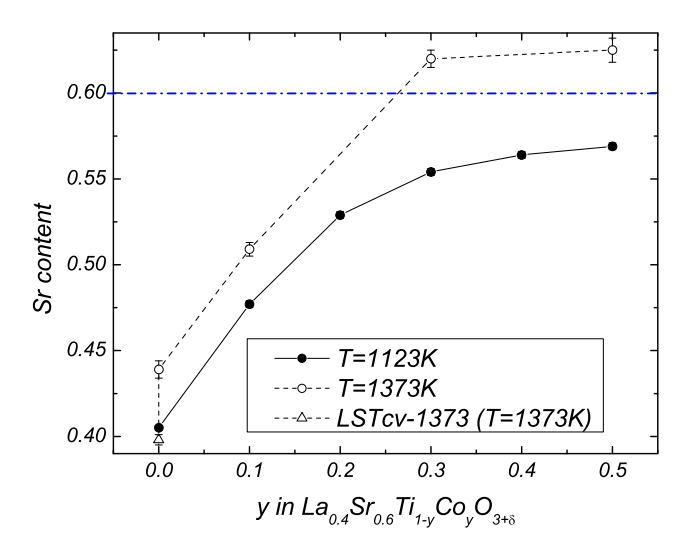


Fig. 5 – Strontium occupation dependency with cobalt content in $\text{La}_{0.4}\text{Sr}_{0.6}\text{Ti}_{1-y}\text{Co}_y\text{O}_{3+\delta}$ compounds synthesized at 1123 and 1373 K, calculated from Rietveld refinements.

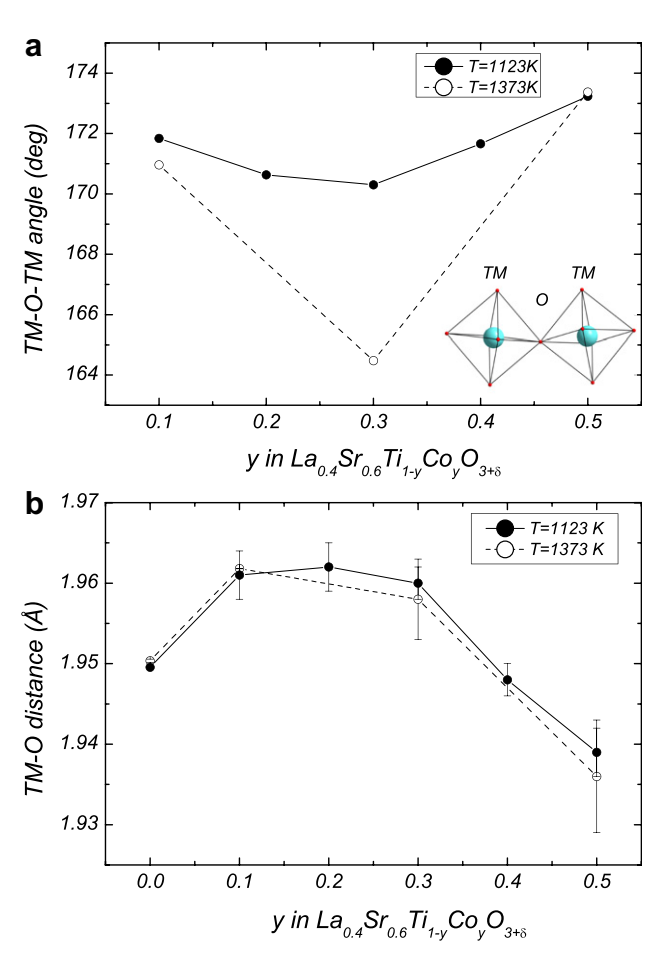


Fig. 6 – Dependence of (a) structural distortion and (b) TM-O distance with Co content for LSTC samples with $0.1 \le y \le 0.5$. The rhombohedral distortion was followed through TM – O – TM angle parameter obtained from Rietveld refinements. (TM: Transition metal).

variation on 1123 K samples is observed, starting from 171.8° (y = 0.1) and ending at 173.2° (y = 0.5), having a distortion maximum at y = 0.3 with 170.3°. On the other hand, a stronger variation is observed on 1373 K samples, also having the maximum distortion level on the corresponding y = 0.3 sample with 164.5°.

It is expected that lower symmetry may result in poorer transport properties. However, atomic distances and possible oxygen diffusion paths may be taken into account to see influence of the distortion in electronic or ionic properties. We found that TM-O distance slightly increases for $0.1 \le y \le 0.3$, but clearly decreases for y > 0.3, which should improve the electronic conductivity with Co doping (see Fig. 6b). On the

other hand, the ratio of the space that may be limiting the oxygen diffusion tends to decrease for y > 0.3. This may result in a compromise for the best doping level to improve the electrochemical properties.

3.2. TEM observations

To investigate the origin of the background signal observed in XPD patterns, transmission electron microscope (TEM) images were acquired from LST-1373 and LSTcv-1373 samples. Bright field images of both powders are shown at Fig. 7a and d, respectively. Grain sizes were calculated as the particle largest dimension and the corresponding histograms are shown in

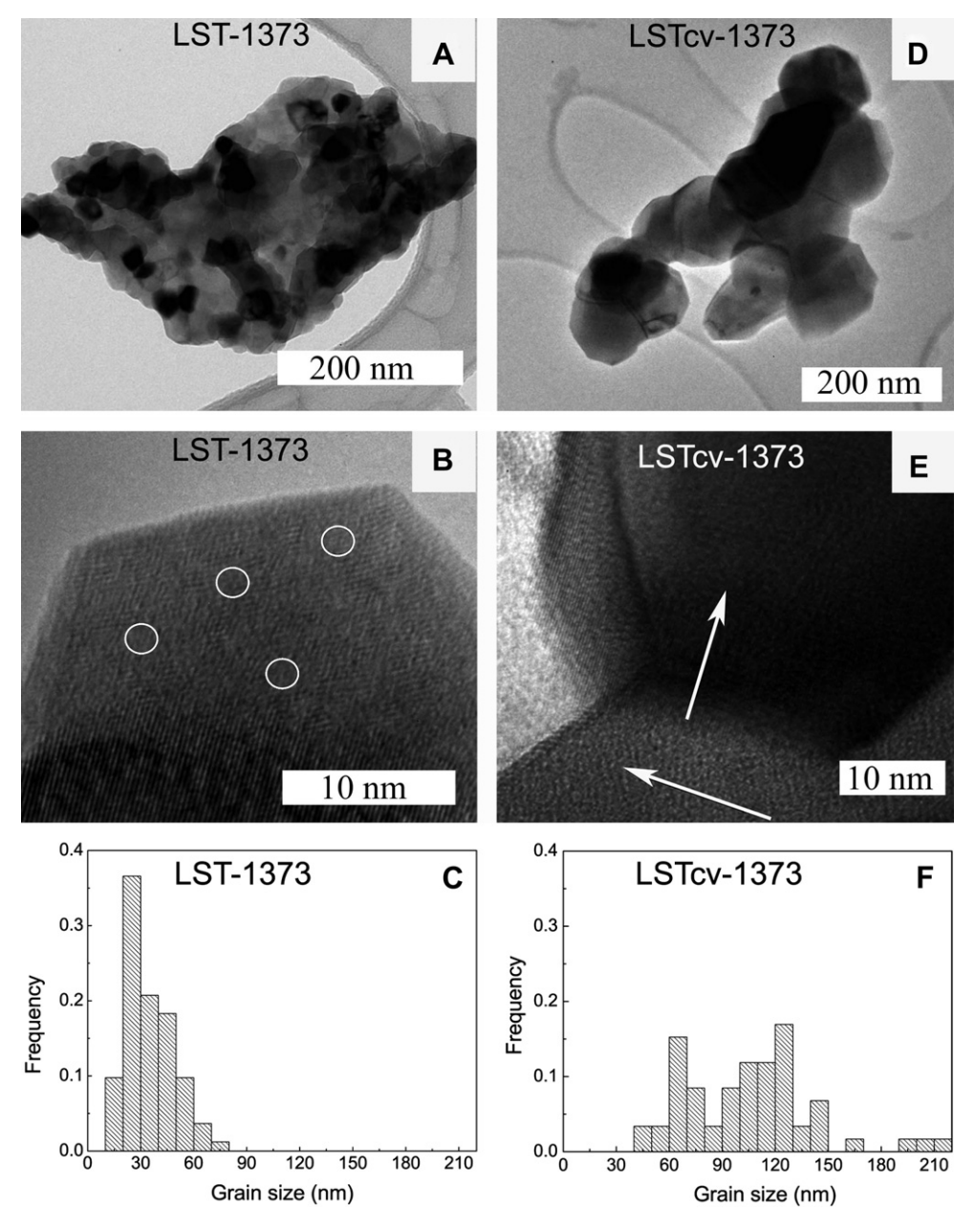


Fig. 7 – Bright field, high resolution TEM images and grain size distribution from y = 0.0 samples synthesized at 1373 K. Prepared as $La_{0.4}Sr_{0.6}TiO_3$ (LST-1373 sample, left) where regions with atomic ordering loss is remarked and as $La_{0.4}Sr_{0.4}TiO_3$ (LSTcv-1373 sample, right).

Fig. 7c and f (50 < N < 100 particles). Although both groups were synthesized at the same temperature, particles synthesized without taking into account in the stoichiometric calculation the A-vacancy site compensation mechanism model (LST-1373) present smaller crystallite sizes than those where the stoichiometry was calculated according to it (LSTcv-1373). The latter group show in addition a wider histogram of sizes and it was possible to identify even some very large (~ 200 nm) well crystallized grains.

Besides, TEM images in high resolution mode (HR-TEM) demonstrate that this group presents perfectly ordered crystals, with well defined atomic planes continuing until the grain border (Fig. 7d), while the notably smaller LST-1373 particles show a combination of well and poor crystallized zones (Fig. 7a and b). As an example, the disruption of some atomic planes inside an individual grain was marked in Fig. 7b: regions within the circles show no particular atomic ordering. This local crystallinity loss is observed, although not in all the particles, in many of them, homogeneously distributed in the whole sample. No additional features, which would correspond to independent amorphous phases, were recognized in our observations. Thus, the mentioned ordering loss seems to be the only cause of the amorphous background signal observed in the XPD analysis of this sample and may be attributed to the disorder caused by Sr segregation.

4. Conclusions

Perovskite-type $\text{La}_{0.4}\text{Sr}_{0.6}\text{Ti}_{1-y}\text{Co}_y\text{O}_{3+\delta}$ oxides with $0.0 \leq y \leq 0.5$ (LSTC), interesting candidates for symmetrical fuel cell electrodes, were synthesized by a low-temperature chemical route decreasing the phase formation temperature in, at least, 300 K compared to previous works reported in the literature. The as-synthesized LSTC powders were characterized by X-ray powder diffraction and Rietveld method refinement, showing cubic $Pm\overline{3}m$ space group for y=0.0 and rhombohedral $R\overline{3}c$ one for $0.1 \leq y \leq 0.5$.

Perovskite A-site vacancies creation was verified as the dominant charge compensation mechanism in LST samples, in agreement with a previous study on a low temperature synthesis route [8,11].

A decrease in the A-site vacancies concentration was observed with the incorporation of Co in the structure, which can be correlated to lattice parameter evolution with Co content. Therefore, the presence of Co, which can be more easily reduced than Ti, precludes the formation of A-site vacancies, even at low synthesis temperature. Correspondingly, the cubic (or pseudocubic) lattice parameter remains stable while this mechanism is still active ($y \le 0.3$) and linearly decreases following a Vegard's law behavior for higher Co proportions.

No significant differences on lattice parameters were found comparing samples synthesized at 1123 and 1373 K. Although same dependence in perovskite A-site vacancies concentration and structural distortion level were observed between both sample series, the charge compensation mechanism shift was favored and the structural distortion level was increased in higher synthesis temperature series.

The increase of the background level observed for diffractograms corresponding to samples with $y \leq 0.3$ could be related to the differences on grain internal ordering clearly observed on HRTEM images. Grain internal disorder and the greatest background increase were observed on y=0.0 sample prepared without compensated vacancies (LSTcv-1373), while these features were absent on LST sample prepared with compensated vacancies.

Acknowledgements

The authors thank Laura Baqué for her support at LNLS measurements and useful discussion, also to Horacio Troiani for his collaboration with TEM observations. This work was funded by UNCuyo, CNEA, CONICET, ANPCyT and particularly LNLS (proposal XPD-11737 at D10B-XPD beamline).

Appendix A. Supplementary data

Supplementary data related to this article can be found at http://dx.doi.org/10.1016/j.ijhydene.2012.09.052.

REFERENCES

- Adler SB. Factors governing oxygen reduction in solid oxide fuel cell cathodes. Chemical Reviews 2004;104(10):4791-843.
- [2] Cowin PI, Petit CTG, Lan R, Irvine JTS, Tao S. Recent progress in the development of anode materials for solid oxide fuel cells. Advanced Energy Materials 2011;1(3):314–32.
- [3] Ruiz-Morales JC, Canales-Vázquez J, Peña Martínez J, Marrero-López D, Núñez P. On the simultaneous use of La_{0.75}Sr_{0.25}Cr_{0.5}Mn_{0.5}O₃-d as both anode and cathode material with improved microstructure in solid oxide fuel cells. Electrochimica Acta 2006;52(1):278–84.
- [4] Ruiz-Morales JC, Marrero-López D, Canales-Vázquez J, Irvine JTS. Symmetric and reversible solid oxide fuel cells. RSC Advances 2011;1(8):1403-14.
- [5] Marina OA, Canfield NL, Stevenson JW. Thermal, electrical, and electrocatalytical properties of lanthanum doped strontium titanate. Solid State Ionics 2002;149(1–2):21–8.
- [6] Lee S, Kim G, Vohs JM, Gorte RJ. Sofc anodes based on infiltration of La_{0.3}Sr_{0.7}Tio₃. Journal of the Electrochemical Society 2008;155(11):B1179–83.
- [7] Canales-Vázquez J, Ruiz-Morales JC, Marrero-López D, Peña Martínez J, Núñez P, Gómez-Romero P. Fe-substituted (La, Sr) Tio₃ as potential electrodes for symmetrical fuel cells (sfcs). Journal of Power Sources 2007;171(2):552-7.
- [8] Eror NG, Balachandran U. Self-compensation in lanthanumdoped strontium titanate. Journal of Solid State Chemistry 1981;40(1):85-91.
- [9] Howard SA, Yau JK, Anderson HU. Structural characteristics of $\rm Sr_{1-x}La_xTi_{3+delta}$ as a function of oxygen partial pressure at 1400° C. Journal of Applied Physics 1989;65(4):1492–8.
- [10] Higuchi M, Aizawa K, Yamaya K, Kodaira K. Electrical properties of $Sr_{1-x}La_xTio_3$ ($0 \le x \le 0.10$) single crystals grown by the floating zone method. Journal of Solid State Chemistry 1991;92(2):573–7.
- [11] Hashimoto S, Kindermann L, Poulsen FW, Mogensen M. A study on the structural and electrical properties of

- lanthanum doped strontium titanate prepared in air. Journal of Alloys and Compounds 2005;397(1–2):245–9.
- [12] Ruddlesden SN, Popper P. The compound $Sr_3Ti_2O_7$ and its structure. Acta Crystallographica 1958;11(1):54–5.
- [13] Canales-Vázquez J, Smith MJ, Irvine JTS, Zhou W. Studies o the reorganization of extended defects with increasing n in the perovskite-based $\text{La}_4\text{Sr}_{n-4}\text{Tino}_{3n+2}$ series. Advanced Functional Materials 2005;15(6):1000–8.
- [14] Li X, Zhao H, Gao F, Chen N, Xu N. La and Sc co-doped $SrTio_3$ as novel anode materials for solid oxide fuel cells. Electrochemistry Communications 2008;10(10):1567–70.
- [15] Fix T, Liberati M, Aubriet H, Sahonta SL, Bali R, Becker C, et al. Ferromagnetism in co-doped (La, Sr)Tio₃. New Journal of Physics 2009;11:073042.
- [16] Yang J, Lee YP, Lee BW. Structural and magnetic properties of spin-and charge-doped Sr_{0.8}La_{0.2}Ti_{0.9}Co_{0.1}O₃. Applied Physics Letters 2007;91(5):052502.
- [17] Yoo KB, Choi GM. Co-doped La_{0.2}Sr_{0.8}Tio₃ as a possible anode for the LaGao₃-based solid oxide fuel cell. ECS Transactions 2009;25:2259–66.
- [18] Li X, Zhao H, Xu N, Zhou X, Zhang C, Chen N. Electrical conduction behavior of La, Co Co-doped SrTio₃ perovskite as anode material for solid oxide fuel cells. International Journal of Hydrogen Energy 2009;34(15):6407−14.
- [19] Shen Y, Wang F, Ma X, He T. SrCo1-yTi_yO3- as potential cathode materials for intermediate-temperature solid oxide fuel cells. Journal of Power Sources 2011;196(18):7420-5.
- [20] Imada M, Fujimori A, Tokura Y. Metal-insulator transitions. Reviews of Modern Physics 1998;70(4):1039–263 [rMP].

- [21] Mao C, Dong X, Zeng T. Synthesis and characterization of nanocrystalline barium strontium titanate powders prepared by citrate precursor method. Materials Letters 2007; 61(8–9):1633–6.
- [22] Ferreira FF, Granado E, Carvalho Jr W, Kycia SW, Bruno D, Droppa Jr R. X-ray powder diffraction beamline at d10b of lnls: application to the Ba₂FeReO₆ double perovskite. Journal of Synchrotron Radiation 2006;13(1):46-53.
- [23] Rietveld H. Line profiles of neutron powder-diffraction peaks for structure refinement. Acta Crystallographica 1967;22(1): 151–2.
- [24] Rodríguez-Carvajal J. Recent advances in magnetic structure determination by neutron powder diffraction. Physica B: Condensed Matter 1993;192(1-2):55-69.
- [25] Dwivedi RK, Parkash O, Christopher CC, Kumar D, Pandey L. Effect of processing route and parameters on the dielectric properties of the valence compensated composition Sr_{0.65}La_{0.35}Ti_{0.65}Co_{0.35}O₃. Journal of Materials Science Letters 1996;15(21):1865-7.
- [26] Battle PD, Bennett JE, Sloan J, Tilley RJD, Vente JF. A-site cation-vacancy ordering in Sr_{1-3x/2}La_xTio₃: a study by hrtem. Journal of Solid State Chemistry 2000;149(2): 360-9
- [27] Boultif A, Louer J. Powder pattern indexing with the dichotomy method. Journal of Applied Crystallography 2004; 37:724—31.
- [28] Closset NMLNP, Van Doorn RHE, Kruidhof H, Boeijsma J. About the crystal structure of La1-xSrxCoO₃-O₃- (0x0.6). Powder Diffraction 1996;11(1):31-4.